TẠP CHÍ KHOA HỌC
TRƯỜNG ĐẠI HỌC QUY NHƠN

Tăng cường khả năng bắt giữ khí SO_2 của $M_2(BDC)_2TED$ (M = Mg, V, Co, or Ni) bằng nghiên cứu tính toán

Nguyễn Quang Vinh[1], Nguyễn Trương Mỹ Duyên[2], Nguyễn Lê Bảo Trân[1], Nguyễn Văn Nghĩa[1], Lê Thị Thảo Viễn[1], Huỳnh Thị Minh Thành[1], Nguyễn Thị Xuân Huynh[1,*]

[1]Khoa Khoa học Tự nhiên, Trường Đại học Quy Nhơn, Việt Nam
[2]Trung tâm Khám phá khoa học và Đổi mới sáng tạo, Việt Nam

Ngày nhận bài: 02/12/2023; Ngày sửa bài: 03/02/2024;
Ngày nhận đăng: 05/02/2024; Ngày xuất bản: 28/02/2024

TÓM TẮT

Cùng với việc phát triển các nguồn năng lượng sạch bền vững thì bảo vệ môi trường là vấn đề rất cấp thiết vì ô nhiễm không khí. Trong đó, SO_2 ảnh hưởng nghiêm trọng đến sức khỏe con người. Do đó, việc loại bỏ SO_2 làm sạch môi trường vô cùng cấp bách. Đã có rất nhiều công nghệ được đề xuất để giải quyết vấn đề này nhưng chưa thực sự hiệu quả. Sự nổi lên của vật liệu xốp có bề mặt riêng và tính xốp cực lớn đã thu hút nghiên cứu bắt giữ SO_2. Trong đó, vật liệu khung hữu cơ kim loại rất được quan tâm trong hấp phụ, tách lọc và một số ứng dụng tiềm năng khác. Trong nghiên cứu này, nhóm $M_2(BDC)_2TED$ (M = Mg, V, Co, Ni) được chọn để nghiên cứu khả năng bắt giữ SO_2 bằng phương pháp mô phỏng tại 298 K và áp suất đến 2,5 bar. Kết quả chỉ ra lượng SO_2 hấp phụ trong $M_2(BDC)_2(TED)$ (or M-MOF) theo thứ tự: Co < Ni < V < Mg. Tại 298 K và 2,5 bar, lượng hấp phụ SO_2 lớn nhất với 16 mmol/g cho Mg-MOF và 13 – 14 mmol/g cho các M-MOF còn lại. Nghiên cứu cũng làm sáng tỏ các yếu tố làm tăng cường hấp phụ SO_2 trong M-MOF gồm nhiệt hấp phụ, diện tích bề mặt riêng (SSA) và thể tích rỗng (V_p). Kết quả cho thấy khả năng bắt giữ SO_2 tăng gần tuyến tính theo SSA và V_p. Hơn nữa, bản chất tương tác giữa các DOS của SO_2 với $M_2(BDC)_2(TED)$ cũng được làm sáng tỏ. Các DOS của SO_2 chủ yếu tương tác với quỹ đạo *p* của C và O trong M-MOF ở dưới mức Fermi.

Từ khóa: MOFs *$M_2(BDC)_2TED$, bắt giữ SO_2, hấp phụ SO_2, diện tích bề mặt riêng, thể tích rỗng.*

**Tác giả liên hệ chính.*
Email: nguyenthixuanhuynh@qnu.edu.vn

QUY NHON UNIVERSITY
JOURNAL OF SCIENCE

Computational study on enhancing SO_2 capture capacity of $M_2(BDC)_2TED$ (M = Mg, V, Co, or Ni)

Nguyen Quang Vinh[1], Nguyen Truong My Duyen[2], Nguyen Le Bao Tran[1], Nguyen Van Nghia[1], Le Thi Thao Vien[1], Huynh Thi Minh Thanh[1], Nguyen Thi Xuan Huynh[1,*]

[1]Faculty of Natural Sciences, Quy Nhon University, Vietnam
[2]Explora Science Quy Nhon, Vietnam

Received: 02/12/2023; Revised: 03/02/2024;
Accepted: 05/02/2024; Published: 28/02/2024

ABSTRACT

Along with finding and developing sustainable clean energy sources, environmental protection is highly urgent because the air is increasingly polluted by more and more toxic gases. In particular, the presence of toxic gas SO_2 seriously affects human health. Therefore, removing toxic SO_2 gas to clean the living environment is extremely urgent. Many technologies have been suggested to solve this, but they have not been effective yet. In recent years, the emergence of porous materials with ultra-large specific surface areas and ultra-high porosity has attracted the attention of scientists in SO_2 capture. Among porous materials, metal-organic frameworks are intensely interested in adsorption, separation, and other potential applications. Herein, we select the porous materials $M_2(BDC)_2TED$ (M = Mg, V, Co, Ni) to study the SO_2 capture using simulation approaches. The research was performed at room temperature 298 K and pressure under 2.5 bar. Our results show that the order of metals gradually increasing the SO_2 adsorption uptake in $M_2(BDC)_2(TED)$ is Co < Ni < V < Mg. Specifically, at 298 K and 2.5 bar, the amount of SO_2 adsorption is about 16 mmol/g for Mg-MOF, and about 13 – 14 mol/g for the M-MOF (M = V, Ni, Co). The study also elucidated the influencing factors that enhance SO_2 adsorption in $M_2(BDC)_2TED$, including adsorption isosteric heat, specific surface area, and pore volume. Noticeably, the specific surface areas and pore volumes of M-MOFs almost linearly enhance the SO_2 capture capability at room temperature and low pressure. Furthermore, we also elucidate the orbital interaction nature between SO_2 and $M_2(BDC)_2(TED)$ MOFs in detail. Therein, the DOS peaks of the SO_2 adsorbate mainly interact with the adsorbents' C and O p orbitals below the Fermi level.

Keywords: *$M_2(BDC)_2TED$ MOFs, SO_2 capture, SO_2 adsorption, specific surface area, pore volume.*

1. INTRODUCTION

Sulfur dioxide (SO_2) is a colorless, non-flammable, and common pollutant in industrial production as well as daily life. Exposure to SO_2 may irritate the nose, throat, and eyes. Besides, SO_2 is a corrosive gas with high solubility (120 g/L) in water and can combine with water and air to form sulfuric acid, the main component of acid rain.[1,2,3] Despite the low SO_2 content in the air, it is classified as a toxic gas and one of the six most common environmental pollutants by the US Environmental Protection Organization.[4] Notably, significant amount of sulfur oxides (SO_x), especially SO_2, is released into the environment after the combustion of petroleum-based fuels

**Corresponding author.*
Email: nguyenthixuanhuynh@qnu.edu.vn

https://doi.org/10.52111/qnjs.2024.18108

in internal combustion engines utilized in motorized vehicles.[3] Therefore, removing or reducing the quantities of SO_2 in the atmosphere is exceptionally urgent. In technologies, SO_2 capture based on the adsorption mechanism has been remarkable.[5] Metal-organic frameworks (MOFs) among porous materials are an exciting alternative for SO_2 capture due to outstanding structural properties such as ultrahigh surface area, high porosity, and controllable structural characteristics.[2,4] Therefore, SO_2 capture in nano-porous materials has attracted scientific interest. Many MOFs and other porous candidates have been studied and highly appreciated for SO_2 adsorption. Fu and co-workers showed that functionalized covalent triazine framework (CTF–CSU41) achieved the highest uptake of SO_2 with a maximum capacity of 6.7 mmol/g (*i.e.*, 42.9 wt.%) at (298 K, 0.15 bar).[3,6] For MOFs, MOF-177 exhibited the highest SO_2 uptake with 25.7 mmol/g at (293 K, 1 bar). Some other MOFs also showed high SO_2 capture capacity, ranging from 4.8 to 17.3 mmol/g.[3] Besides many other MOFs, $M_2(BDC)_2(TED)$ or $M(BDC)(TED)_{0.5}$ materials have been attractive for applications in capturing toxic gases (CO_2, SO_2, CH_4, NH_3, H_2S, NO_x, …).[4] In this research, we use simulations to find optimum $M_2(BDC)_2(TED)$ MOFs for SO_2 capture, where M is magnesium (Mg), vanadium (V), cobalt (Co) or nickel (Ni); BDC = 1,4-Benzenedicarboxylate; TED = Triethylen-diamine or DABCO: 1.4-Diazabicyclo [2.2.2] octane.[7]

2. COMPUTATIONAL METHODS

The research approach combines density functional theory (DFT) calculations and grand canonical Monte Carlo (GCMC) simulations. Firstly, we used DFT calculations to optimize the geometries of $M_2(BDC)_2(TED)$ MOFs, namely M-MOFs. Secondly, GCMC simulations were used to obtain the isotherms and isosteric heat of SO_2 adsorption as well as calculate the structural characteristics of the M-MOFs.

To optimize the unit cell, extract partial atomic charges of the M-MOFs, search stable or favourite adsorption sites and DOS/PDOS, we utilized the Vienna ab initio simulation package (VASP)[8,9] for the van der Waals dispersion-corrected density functional theory (vdW-DF).[10,11] The plane-wave basis set with the cut-off energy of 700 eV for the plane-wave basis set.[12,13] We performed the surface Brillouin-zone integrations using the Monkhorst and Pack *k*-point sampling technique with the 3×3×3 mesh grid and the Gamma point at the center.[14] The Methfessel-Paxton smearing of order 1 was used for the ions and geometry relaxation, and atomic charge calculation with the smearing width sigma of 0.1 eV.[15]

GCMC simulations using the RASPA code were selected to study the gravimetric uptakes of SO_2 in the M-MOFs.[16] These simulations were performed in constant volume, temperature, and chemical potential at room temperature (298 K) and pressures up to 2.5 bar. The number of 300000 MC steps were simulated for the random insertion, deletion, translation, and rotation of SO_2 molecules in the simulation box, repeated 3×3×3 times of the primary unit cell along the *a*, *b*, and *c* lengths.

The interactions between atoms of SO_2 gas and the MOFs were described by (*i*) the Coulombic or electrostatic interactions with its cut-off radius of 13 Å, and (*ii*) the van der Waals interactions with the simple Lennard-Jones (LJ) model with the LJ cut-off radius of 20 Å.[17,18] The cut-off radius and other parameters were carefully checked before performing the GCMC simulation. The partial charges of atoms of the M-MOFs were extracted from the density-derived electrostatic and chemical (DDEC6 atomic charges method, listed in Table 1, with the symbols for the atoms shown in Figure 1.[19–22] The qualities of the LJ potential well depth and diameter were determined by the Lorentz–Berthelot combining rules, one of the most common types of mixing rules for unlike atoms.[23,24] The parameters for σ_i and ε_i (*i* refers to the atoms like Fe, H, C, O in the M-MOFs or S, O in SO_2) were selected from the generic

force fields for MOFs in the RASPA software package.[16,25]

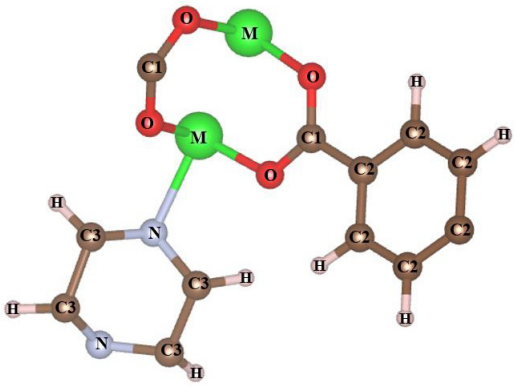

Figure 1. The symbol for atomic types with different charges of M-MOFs.

Table 1. The LJ (ε, σ) and charge parameters (q) for atomic types of M-MOFs and SO_2.

M-MOFs	Atomic types	LJ parameters		q (e)
		ε/kg (K)	σ (Å)	
M = Mg	C1	47.856	3.472	0.739
	C2			-0.073
	C3			0.011
	H	7.648	2.846	0.088
	N	38.949	3.262	-0.362
	O	48.158	3.033	-0.721
	Mg	**55.857**	**2.691**	**1.385**
M = V	C1	47.856	3.472	0.627
	C2			-0.073
	C3			-0.012
	H	7.648	2.846	0.076
	N	38.949	3.262	-0.174
	O	48.158	3.033	-0.574
	V	**8.051**	**2.801**	**0.926**
M = Co	C1	47.856	3.472	0.613
	C2			-0.071
	C3			-0.025
	H	7.648	2.846	0.076
	N	38.949	3.262	-0.099
	O	48.158	3.033	-0.491
	Co	**7.045**	**2.558**	**0.573**
M = Ni	C1	47.856	3.472	0.636
	C2			-0.071
	C3			-0.025
	H	7.648	2.846	0.079
	N	38.949	3.262	-0.118
	O	48.158	3.033	-0.539
	Ni	**7.548**	**2.524**	**0.660**
SO_2[25,26]	O	58.725	3.198	-0.201
	S	189.353	3.410	0.402

In this work, to search the stable or favorite adsorption sites of SO_2 gas in $M_2(BDC)_2(TED)$, we calculated the adsorption energy of SO_2 gas in the $M_2(BDC)_2TED$ series by the expression $\Delta E = E_{(M\text{-}MOF+SO_2)} - (E_{M\text{-}MOF} + E_{SO_2})$. Where $E_{(M\text{-}MOF+SO_2)}$, $E_{M\text{-}MOF}$, and E_{SO_2} are the total energies of the [M - MOF + SO_2] system, the pristine $M_2(BDC)_2TED$ MOF, and the isolated SO_2 molecule, respectively.

3. RESULTS AND DISCUSSION

3.1. Optimization of the unit cell of $M_2(BDC)_2(TED)$

First, we constructed a unit cell based on experimental and computational works for $Ni_2(BDC)_2(TED)$ (BDC = Benzene dicarboxylate, and TED = Triethylenediamine) (Figure 2).[7,27] We optimized all ions and the size of the unit cells. Then, we replaced Ni with other bivalent metals such as Mg, V, and Co, which often appear in MOFs and greatly influence gas adsorption. The results obtained for the unit cells are listed in Table 2 and compared with the experimental data for M = Ni,[28] showing that these optimal results show reliability with 1.61%, 1.57%, and 4.81% for a (or b), c lengths, and the cell volume. The unit cell volume ($V_{M\text{-}MOF}$) of the M-MOFs also does not change much, and they are in slightly increasing order: $V_{Co\text{-}MOF} < V_{V\text{-}MOF} \approx V_{Ni\text{-}MOF} < V_{Mg\text{-}MOF}$.

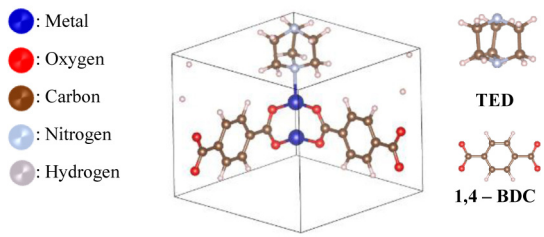

Figure 2. A primary unit cell of M-MOFs (M = Mg, V, Co or Ni).

https://doi.org/10.52111/qnjs.2024.18108

Table 2. The optimized parameters of the unit cell of the $M_2(BDC)_2TED$ structures, compared with other works.

$M_2(BDC)_2TED$	Lattice constant (Å)		Volume of unit cell (Å³)
	a = *b*	*c*	
M = Mg	10.98	9.39	1130
M = V	10.96	9.37	1125
M = Co	10.90	9.31	1113
M = Ni	10.97	9.38	1128
M = Ni (exp. data)[28]	11.15	9.53	1185
Error compared exp. data (%)	1.61	1.57	4.81

3.2. The SO_2 capture capability of $M_2(BDC)_2TED$ MOFs

The SO_2 adsorption isotherms are shown in Figure 3 for both excess and absolute uptakes at pressures up to 2.5 bar. The results show these two uptakes are nearly similar for SO_2 on the M-MOFs (M = Mg, V, Co, or Ni) at low pressure under 2.5 bar. The adsorption uptakes for all metals are listed in Table 3. Our data are also compared to other ones. Compared to MOF-177, the best SO_2 capture to date, M-MOFs strongly adsorb SO_2 at low pressure below 0.5 bar.[1] On the contrary, above 0.5 bar, MOF-177 shows an outstanding uptake compared to our M-MOFs and other MOFs.[1]

The adsorption tendency in Mg-MOF is more substantial than in Ni-MOF, which is consistent with the experimental data of Kui Tan et al. at the same temperature and pressure conditions (0.11 bar, 298 K),[7] and and V. B. López-Cervantes et al (Table 3).[29,30]

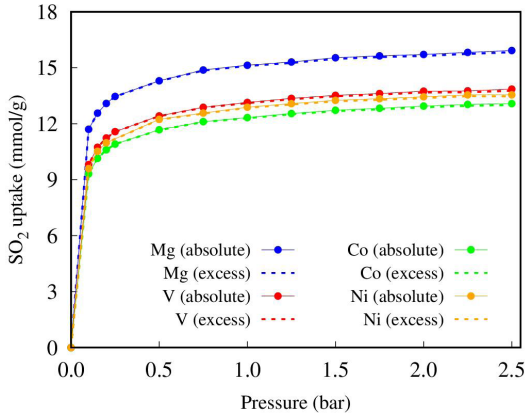

Figure 3. Absolute and excess isotherms of SO_2 on $M_2(BDC)_2(TED)$ at 298 K, where dashed lines and solid lines refer to absolute and excess uptakes.

Table 3. Absolute and excess SO_2 uptakes on $M_2(BDC)_2(TED)$ at 298 K.

M-MOFs	SO_2 uptakes (mmol/g)		
	0.1 bar	1 bar	2.5 bar
M = Mg	11.69	15.13	15.92
M = V	9.80	13.13	13.85
M = Co	9.31	12.32	13.07
M = Ni	9.59	12.88	13.54
M = Ni[17]			13.6 (50 bar)
M = Mg[7]	6.44 (0.11 bar)	8.60 (1.02 bar)	
M = Ni[7]	4.54 (0.11 bar)	9.97 (1.13 bar)	
Mg(II)-MOF[29]		19.5	
Ni(II)-MOF[30]		12.5	
MOF-177[1,29]	1.3	25.7 (maximum, 293 K, 0.97 bar)	-

In this work, we study the adsorption capacity of M-MOFs for SO_2 up to a pressure of 2.5 bar because researching at high pressures is unnecessary, and the results achieved only change a little.[17] The results show that Mg-MOF has the strongest adsorption of SO_2, followed by V-MOF, Ni-MOF, and Co-MOF. Here, Mg-MOF adsorbs superiorly compared to the remaining M-MOFs (M = V, Ni, Co). At 2.5 bar and 298 K, the best uptakes reach for Mg-MOF with n_{exc}=15.82mmol/g,n_{abs}=15.92mmol/g, followedby V-MOF (n_{exc} = 13.77 mmol/g, n_{abs} = 13.85 mmol/g), Ni-MOF (n_{exc} = 13.46 mmol/g, n_{abs} = 13.54 mmol/g), and Co-MOF (n_{exc} = 13.00 mmol/g, n_{abs} = 13.08 mmol/g).

3.3. Effect of structural characteristics and isostericheat on the SO_2 adsorption of $M_2(BDC)_2(TED)$

To explain the reason Mg increases the ability to capture SO_2 based on the adsorption mechanism compared to other metals, we analyze the factors that have a substantial impact on the gas adsorption of MOFs, which are the structural characteristics (specific surface area and pore volume) and adsorption isosteric heat.

Isosteric heat of adsorption, Q_{st}, is an essential factor required to describe the thermal

performance of adsorptive systems.[31] The Q_{st} of SO_2 for the M-MOF series calculated in low pressures under 1.0 kPa are presented in Figure 4. The results show that Q_{st} tends to increase as pressure increases. However, the values change little in the low-pressure region. At higher pressures, the Q_{st} value of SO_2 for M-MOFs is most significant for Mg-MOF, rising from 42.03 kJ/mol to 47.97 kJ/mol. Meanwhile, other M-MOFs increase slightly with pressure. Specifically, uptakes of SO_2 in V-MOF: 40.61 – 44.73 kJ/mol, Co-MOF: 40.93 – 45.37 kJ/mol, and Ni-MOF: 40.78 – 44.94 kJ/mol.

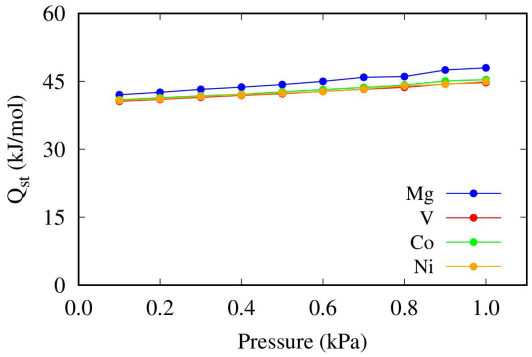

Figure 4. Isosteric heats of SO_2 adsorption for M-MOFs vs the pressure.

The Q_{st} value of SO_2 adsorption is in the order V-MOF ≈ Ni-MOF ≈ Co-MOF < Mg-MOF, exhibiting that SO_2 adsorption on $Mg_2(BDC)_2(TED)$ is the most noticeable as analyzed above. Moreover, we also research the influence of specific surface area (SSA) and pore volume (V_p) on the adsorptive ability of SO_2 on the M-MOFs. The SSA values are smaller than many other MOFs, but the pore volume is relatively large, as detailed in Table 4. The SSA and pore volume of the M-MOFs are in increasing order Co < Ni < V < Mg. This tendency is consistent with H. Xiang's work for $M(BDC)(TED)_{0.5}$ with M is Ni and Co.[32]

Table 4. The specific surface area and the pore volume of $M_2(BDC)_2(TED)$, compared to another work.

M-MOFs	This work		H. Xiang[32]	
	SSA (m^2/g)	V_p (cm^3/g)	SSA (m^2/g)	V_p (cm^3/g)
M = Mg	1930.95	0.87	-	-
M = V	1727.18	0.78	-	-
M = Co	1627.58	0.74	1708	0.619
M = Ni	1686.09	0.76	1905	0.757

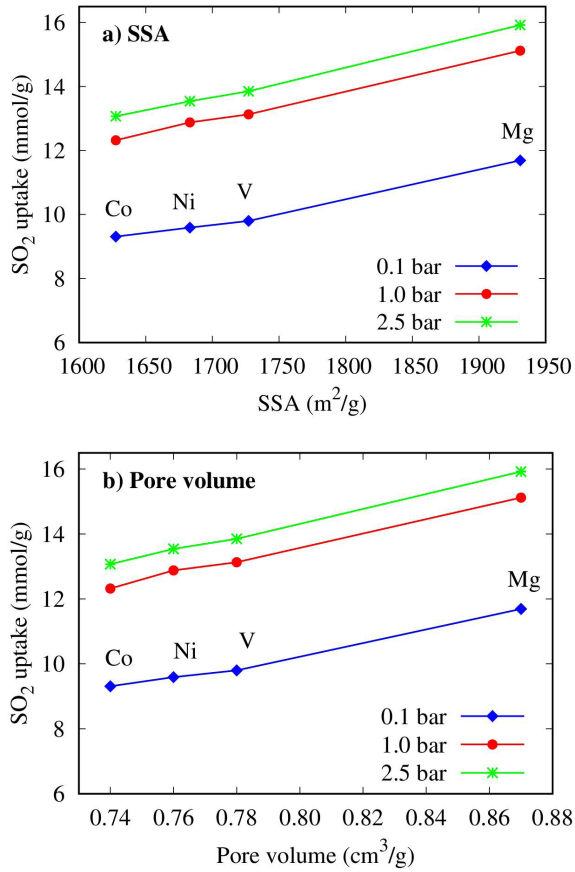

Figure 5. The correlation between the uptakes and (a) the specific surface area (SSA), (b) pore volume (Vp) of $M_2(BDC)_2(TED)$ at 298 K.

The results in Figure 5 express that the amounts of SO_2 adsorption increase almost entirely linearly with SSA and V_p. Among them, the M-MOF with M = Mg is outstanding, which explains the most excellent SO_2 adsorption into $Mg_2(BDC)_2(TED)$. Therefore, these two structural characteristics (V_p and SSA) have a powerful impact on the ability to capture SO_2 on MOFs at room temperature.

3.4. Nature of interaction between SO_2 and $M_2(BDC)_2(TED)$ at the electronic orbital level

GCMC simulation results give us quantitative numbers, results that can be compared with experiments and evaluate the relative adsorption strength of the M-MOFs by changing their metals. Therefore, to clarify the nature of the interaction between SO_2 and M-MOFs, we perform further calculations on the electronic structure through DFT calculations.

https://doi.org/10.52111/qnjs.2024.18108

We indicate the preferential SO_2 adsorption in M-MOFs (M = Mg, V, Co, Ni). In this work, the effect of metals on SO_2 adsorption on the M-MOF is of interest; Therefore, we only search for stable SO_2 adsorption sites near the metal of the MOF. Therefore, we only search for stable SO_2 adsorption sites near the metal of the MOF by evaluating adsorption energies. The values of SO_2 adsorption energies on the M-MOFs are shown in Table 5 and Figure 6. Noting that the more negative ΔE, the more stable the adsorption.

Among the selected metals in this research, vanadium (V) indicates the most considerable SO_2 adsorption with the most negative energy value ΔE = -0,62 eV); the remaining metals show the values of ΔE close to each other, in the range of -0.40 to -0.43 eV. Table 5 also shows that the distance between SO_2 and the metal of all M-MOFs has very little difference except V, which has shorter SO_2-V distance. Although V increases the superior adsorption energy compared to other metals, Mg still gives the most substantial SO_2 adsorption on the $Mg_2(BDC)_2(TED)$. These results exhibit a significant and decisive influence on structural characteristic quantities such as SSA and V_p.

Table 5. Adsorption energy (ΔE) and the distance between the nearest atoms of SO_2 and the M-MOF ($d_{SO_2\text{-}MOF}$).

M-MOF	Adsorption energy, ΔE		($d_{SO_2\text{-}MOF}$)
	(eV)	(kJ/mol)	(Å)
M = Mg	-0.41	-40.21	3.47
M = V	-0.62	-59.91	3.36
M = Co	-0.40	-38.85	3.44
M = Ni	-0.41	-40.45	3.50

To provide further insights into the interaction nature between SO_2 (adsorbate) and M-MOFs (adsorbent), we calculated and analyzed the modification of the total electronic density of states (DOS) and orbital-projected density of states (PDOS) between SO_2 and M-MOFs (M = Mg, V, Co, Ni) for the above favorable SO_2 adsorption systems. First, we analyzed the DOS peaks of isolated SO_2, including $1\sigma^*$, $2\sigma/1\pi/3\sigma$ *2n, 3n, 4n*, and $1\pi^*$ (Figure 7).[27] The results revealed that, after the adsorption of SO_2 on M-MOFs, the adsorbate's DOS peaks shift to the left side of the Fermi level with substantial expansion of the DOS ($2\sigma/1\pi/3\sigma$ and $4n$). There, the total peaks of the SO_2 on M-MOFs with M = Co, Ni, V much stronger shift than those of M = Mg (Figure 7). Notably, V-MOF also causes all DOS peaks of SO_2 to split except the $3n$ peak, which explains the most favorite adsorption of SO_2 in V-MOF compared to the remaining MOFs.

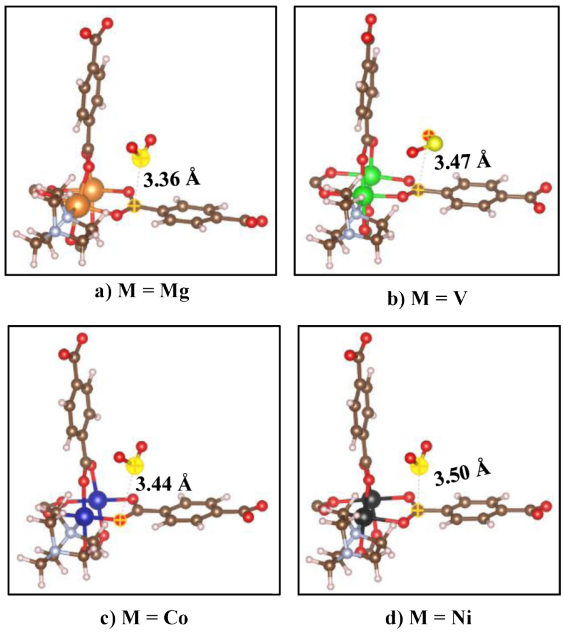

Figure 6. The favorable SO_2 adsorption configurations on $M_2(BDC)_2(TED)$: a) M = Mg, b) M = V, c) M = Co, and d) M = Ni.

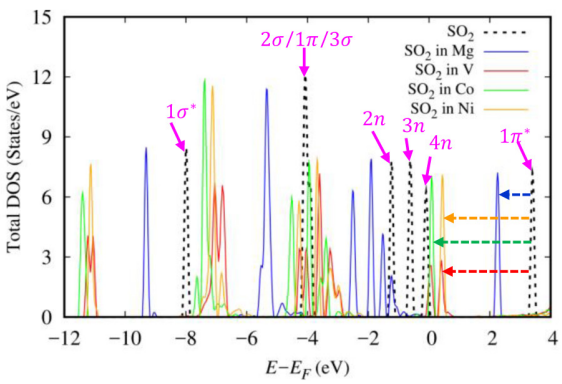

Figure 7. Total DOS of the adsorbed SO_2 in M-MOFs (M = Mg, V, Co or Ni) compared to the isolated SO_2 (black dash line). The Fermi level was set to 0 eV.

Next, the modification of the DOS of the SO_2 molecule and the M-MOF's atoms (C, O, N, and M) was considered (Figure 8). Here, we ignored the weak interaction between H atoms of the MOFs and SO_2. The results indicate that the overlap between the DOS peaks of SO_2 molecule with the majority of C and O *p* orbitals (Figure 8) and a small fraction of M *d* orbitals in M-MOFs (Figure 9) enhances the interaction between the adsorbate and adsorbent. In particular, for $V_2(BDC)_2(TED)$, substantial overlap occurs between SO_2 $1\pi^*$ peak and the M *d* (mainly d_{xz}, d_{yz}, and d_{xy}) orbitals at about 0 eV (Fermi level) compared to other metals. This resonance can explain the most preferred adsorption of SO_2 in V-MOF. In contrast to other metals, Mg shows that the interaction occurs between the C and especially O *p* states of the Mg-MOF with SO_2 $2\sigma/1\pi/3\sigma$ state and N *p* orbitals with SO_2 $2n$ state. Note that we have analyzed the PDOS between SO_2 and the atoms of M-MOFs in detail and discussed the results obtained here despite ignoring some figures.

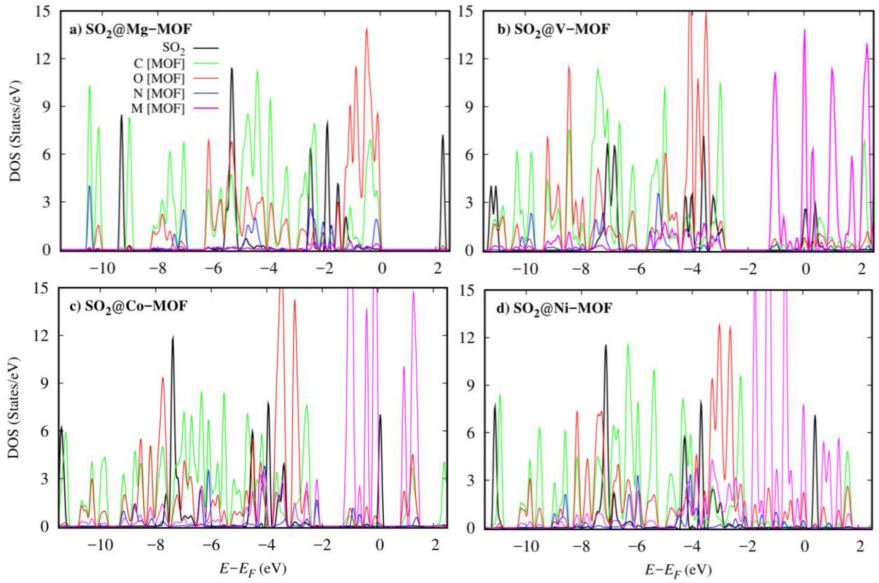

Figure 8. The overlap between DOS of the SO_2 and that of O, N, and M atoms of M-MOFs, where the Fermi level was set to 0 eV: a) SO_2@Mg-MOF, b) SO_2@V-MOF, c) SO_2@Co-MOF, and d) SO_2@Ni-MOF.

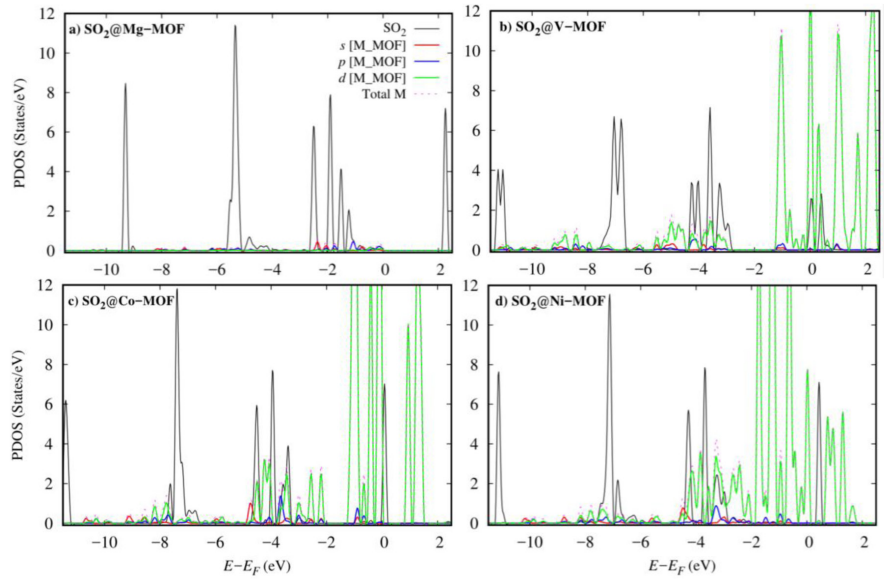

Figure 9. The orbital-projected DOS of the SO_2 with the states (*s*, *p*, *d*) of M atoms of M-MOFs, where the Fermi level was set to 0 eV: a) SO_2@Mg-MOF, b) SO_2@V-MOF, c) SO_2@Co-MOF, and d) SO_2@Ni-MOF.

https://doi.org/10.52111/qnjs.2024.18108

4. CONCLUSION

After optimizing the structure for Ni(BDC)(TED), we replaced the metal to obtain optimized geometries for M(BDC)(TED), with M being Mg, V, and Co by calculations based on vdW-DF. Unit cell volumes are in ascending order of Co < V ≈ Ni < Mg.

The order of metals increasing the SO_2 adsorption uptakes on $M_2(BDC)_2(TED)$ is Co < Ni < V < Mg. At 298 K and 2.5 bar, SO_2 uptakes are about 16 mmol/g for Mg-MOF (n_{exc} = 15.82 mmol/g, n_{abs} = 15.92 mmol/g) and about 13 – 14 mol/g for the M-MOF (M = V, Ni, Co).

Our work also elucidates the factors that enhance the amounts of SO_2 adsorption in $M_2(BDC)_2TED$, including the adsorption isosteric heat, specific surface area, and pore volume. Remarkably, the specific surface areas and pore volumes of M-MOFs almost linearly enhance the SO_2 capture at room temperature and low pressure.

Moreover, the physical insights at electronic orbitals illustrated that the SO_2@ $M_2(BDC)_2(TED)$ interactions are contributed by the C and O *p* orbitals (more predominant) and the metal *d* orbitals (weaker). Therein, the most stable SO_2 adsorption configuration is in $V_2(BDC)_2(TED)$ by the more significant overlap between the V *d* states and the SO_2 orbitals. For SO_2@$Mg_2(BDC)_2(TED)$, the dominant interactions occur between O *p* and C *p* states with $2\sigma/1\pi/3\sigma$ and N *p* with $2n$ of SO_2, respectively.

Acknowledgments

This work was financially supported by the Ministry of Education and Training of Vietnam under the grant number B2022-DQN-05. We also acknowledge supporting the computer time and software granted by the Lab of Computational Chemistry and Modelling (LCCM), Faculty of Natural Sciences, Quy Nhon University, Quy Nhon, Vietnam.

REFERENCES

1. C. Janiak. Metal-organic frameworks with potential application for SO_2 separation and fluegas desulfurization, *ACS Applied Materials & Interfaces*, **2019**, *11*, 17350−17358.
2. E. M. Ahumada, M. L. D. Ramírez, M. D. J. V. Hernández, V. Jancik, I. A. Ibarra. Capture of toxic gases in MOFs: SO_2, H_2S, NH_3 and NO_x, *Chemical Science,* **2021**, *12*, 6772–6799.
3. C. G. Livas, D. Raptis, E. Tylianakis, G. E. Froudakis. Multiscale theoretical study of sulfur dioxide (SO_2) adsorption in metal-organic frameworks, *Molecules*, **2023**, *28*(7), 3122.
4. T. T. T. Huong, P. N. Thanh, N. T. X. Huynh, D. N. Son. Metal – organic frameworks: state-of-the-art material for gas capture and storage, *VNU Journal of Science: Mathematics - Physics*, **2016**, *32*, 67–85.
5. E. M. Ahumada, A. L. Olvera, V. Jancik, J. E. S. Bautista, E. G. Zamora, V. Martis, D. R. Williams, I. A. Ibarra. MOF materials for thecapture of highly toxic H_2S and SO_2, *Organometallics*, **2020**, *39*, 883–915.
6. Y. Fu, Z. Wang, S. Li, X. He, C. Pan, J. Yan, G. Yu. Functionalized covalent triazine frameworks for effective CO_2 and SO_2 removal, *ACS Applied Materials & Interfaces*, **2018**, *10*, 36002–36009.
7. K. Tan, P. Canepa, Q. Gong, J. Liu, D. H. Johnson, A. Dyevoich, P. K. Thallapally, T. Thonhauser, J. Li, Y. J. Chabal. Mechanism of preferential adsorption of SO_2 into two microporous paddle wheel frameworks $M(BDC)(TED)_{0.5}$, *Chemistry of Materials,* **2013**, *25*, 4653–4662.
8. G. Kresse, J. Furthmüller. Efficient iterative schemes for ab initio total-energy calculations using a plane-wave basis set, *Physical Review B*, **1996**, *54*, 11169–11186.
9. G. Kresse, J. Furthmüller. Efficiency of ab-initio total energy calculations for metals and semiconductors using a plane-wave basis set, *Computational Materials Science*, **1996**, *6*, 15–50.
10. J. P. Perdew, J. Chevary, S. Vosko, K. Jackson, M. Pederson, D. Singh, C. Fiolhais. Atoms, molecules, solids, and surfaces: applications of the generalized gradient approximation for exchange and correlation, *Physical Review B*, **1992**, *46*, 6671–6687.

11. J. P. Perdew, K. Burke, M. Ernzerhof. Generalized gradient approximation made simple, *Physical Review Letters*, **1996**, *77*, 3865–3868.

12. P. E. Blöchl. Projector augmented-wave method, *Physical Review B*, **1994**, *50*, 17953–17979.

13. G. Kresse, D. Joubert. From ultrasoft pseudopotentials to the projector augmented-wave method, *Physical Review B*, **1999**, *59*, 1758–1775.

14. J. D. Pack, H. J. Monkhorst. Special points for Brillouin-zone integrations, *Physical Review B*, **1976**, *13*, 5188–5192.

15. M. Methfessel, A. T. Paxton. High-precision sampling for Brillouin-zone integration in metals, *Physical Review B*, **1989**, *40*, 3616–3621.

16. D. Dubbeldam, S. Calero, D. E. Ellis, R. Q. Snurr. RASPA: molecular simulation software for adsorption and diffusion in flexible nanoporous materials, *Molecular Simulation*, **2016**, *42*, 81–101.

17. N. T. X. Huynh, B. T. Duyen, P. T. Tram, T. T. D. Thanh, N. T. M. Duyen. Research on the capture of flue gases of the metal-organic framework $Ni(BDC)(TED)_{0.5}$ by the classical simulation method, *Quy Nhon University Journal of Science*, **2021**, *15*(5), 5–12.

18. N. T. X. Huynh, T. T. Nam, D. N. Son. Evaluation of H_2 and CO_2 adsorption into MIL-88A-Fe by Grand canonical Monte Carlo simulation, *Quy Nhon University Journal of Science*, **2021**, *15*(1), 5–12.

19. T. A. Manz, N. G. Limas. Introducing DDEC6 atomic population analysis: part 1. Charge partitioning theory and methodology, *RSC Advances*, **2016**, *6*, 47771–47801.

20. N. G. Limas, T. A. Manz. Introducing DDEC6 atomic population analysis: part 2. Computed results for a wide range of periodic and nonperiodic materials, *RSC Advances,* **2016**, *6*, 45727–45747.

21. T. A. Manz. Introducing DDEC6 atomic population analysis: part 3. Comprehensive method to compute bond orders, *RSC Advances*, **2017**, *7*, 45552–45581.

22. N. G. Limas, T. A. Manz. Introducing DDEC6 atomic population analysis: part 4. Efficient parallel computation of net atomic charges, atomic spin moments, bond orders, and more, *RSC Advances*, **2018**, *8*, 2678–2707.

23. H. A. Lorentz. Ueber die anwendung des satzes vom virial in der kinetischen theorie der gase, *Annalen der Physik*, **1881**, *248*, 127–136.

24. D. Berthelot. Sur le mélange des gaz, *Comptes Rendus Chimie*, **1898**, *126*, 1703–1855.

25. D. Dubbeldam, K. S. Walton, T. J. H. Vlugt, S. Calero. Design, parameterization, and implementation of stomic force fields for adsorption in nanoporous materials, *Advanced Theory and Simulations,* **2019**, *2*, 1900135.

26. I. M. Martos, A. M. Calvo, J. J. G. Sevillano, M. Haranczyk, M. Doblare, J. B. Parra, C. O. Ania, S. Calero. Zeolite screening for the separation of gas mixtures containing SO_2, CO_2 and CO, *Physical Chemistry Chemical Physics*, **2014**, *16*, 19884–19893.

27. D. N. Son, T. T. Thuy Huong, V. Chihaia. Simultaneous adsorption of SO_2 and CO_2 in an Ni(BDC)(TED)0.5 metal-organic framework, *RSC Advances*, **2018**, *8*, 38648–38655.

28. K. Tan, N. Nijem, P. Canepa, Q. Gong, J. Li, T. Thonhauser, Y. J. Chabal. Stability and hydrolyzation of metal organic frameworks with paddle-wheel SBUs upon hydration, *Chemistry of Materials*, **2012**, *24*, 3153–3167.

29. M. A. Eva, D. W. Kim, W. Mohammad, C. M. Paulina, A. L. Olvera, D. R. Williams, V. Martis, H. A. L. García, S. L. Morales, D. S. Ibarra, G. Maurin, A. I. Ilich, C. S. Hong. Capture and detection of SO_2 by a chemically stable Mg(II)-MOF, *Journal of Materials Chemistry A*, **2022**, *10*, 18636–18643.

30. V. B. L. Cervantes, D. W. Kim, J. L. Obeso, E. M. Ahumada, Y. A. A. Sánchez, E. S. González, C. Leyva, C. S. Hong, I. A. Ibarra, D. S. Ibarra. Detection of SO_2 using a chemically stable Ni(II)-MOF, *Nanoscale*, **2023**, *15*, 12471–12475.

31. I. E. Menshchikov, A. V. Shkolin, E. M. Strizhenov, E. V. Khozina, S. S. Chugaev, A. A. Shiryaev, A. A. Fomkin, A. A. Zherdev. Thermodynamic behaviors of adsorbed methane storage systems based on nanoporous carbon adsorbents prepared from coconut shells, *Nanomaterials*, **2020**, *10*, 1–26.

32. H. Xiang, A. Ameen, P. Gorgojo, F. R. Siperstein, S. M. Holmes, X. Fan. Selective adsorption of ethane over ethylene on $M(BDC)(TED)_{0.5}$ (M = Co, Cu, Ni, Zn) metal-organic frameworks (MOFs), *Microporous and Mesoporous Materials*, **2020**, *292*, 109724.

https://doi.org/10.52111/qnjs.2024.18108